

**An evaluation of a low-cost pole aerial photography (PAP) and structure from motion (SfM) approach for topographic surveying of small rivers**

Fleur Visser<sup>a\*</sup>, Amy Woodget<sup>b</sup>, Andy Skellern<sup>c</sup>, Jake Forsey<sup>d</sup>, Jeff Warburton<sup>e</sup> and Rich Johnson<sup>c</sup>

*<sup>a</sup>School of Science and the Environment, University of Worcester, Worcester, UK;*

*<sup>b</sup>Department of Geography, Loughborough University, Loughborough, UK; <sup>c</sup>Hazard, Risk and Disaster Research Group, Bath Spa University, Bath, UK; <sup>d</sup>Field Dynamics Consultancy, Birmingham, UK; <sup>e</sup>Department of Geography, Durham University, Durham, UK*

\* Corresponding author. Email address: f.visser@worc.ac.uk

# **An evaluation of a low-cost pole aerial photography (PAP) and structure from motion (SfM) approach for topographic surveying of small rivers**

To better understand fluvial forms and processes, geomorphologists have a need for high-resolution fluvial topographic surveys. Continuous data collection approaches such as airborne laser scanning (ALS), terrestrial laser scanning (TLS) and structure from motion (SfM) photogrammetry provide methods to collect such data sets. Comparisons of SfM and laser-based approaches for topographic surveys have demonstrated site-specific benefits and drawbacks. Survey preference is largely dependent on specific project requirements, indicating a need for examples of best practice for different applications. This study demonstrates how pole aerial photography (PAP) provides specific advantages for SfM data collection when mapping the topography of small river corridors. Digital elevation models (DEMs) were created using three different surveying approaches for a 100 m reach of Coledale Beck, a small upland stream in Cumbria, United Kingdom. This included (a) imagery collected from a 5 m telescopic pole processed using SfM photogrammetry, (b) imagery collected using an unmanned aircraft system (UAS), also processed using SfM photogrammetry, and (c) point cloud data collected using a TLS. All three approaches produce DEMs of sufficient quality to enhance our understanding of fluvial forms and processes, with DEM/point cloud resolutions of 0.01 m for the close-range methods (TLS and PAP) and c. 0.02 m for the longer-range UAS method. Overall, TLS mean errors (0.123-0.135 m) are almost twice as large as the UAS and PAP (0.037-0.103 m) errors and the standard deviation is approximately 25% higher. However, results vary significantly for different surface cover types (i.e. vegetated, exposed and submerged surfaces), with TLS outperforming the other approaches for exposed gravel surfaces. Data acquisition rates for the PAP approach are approximately half those of the two other methods (430 m<sup>2</sup>/hour versus 845 and 730 m<sup>2</sup>/hour for PAP, TLS and UAS respectively). When equipment costs and ease of use are taken into consideration, the PAP approach provides an effective way of collecting topographic data from small rivers.

Keywords: river survey, pole aerial photography; UAV (unmanned aerial vehicle); terrestrial laser scanner; bank morphology;

# **1 Introduction**

## ***1.1 Context***

To better understand fluvial forms and processes, geomorphologists have a need for high-resolution fluvial topographic surveys. Conventional high precision point-based observations, for example taken with differential global positioning system (dGPS) or a total-station, have low spatial coverage, which limits use of the data for spatially continuous mapping and modelling purposes (Young 2012). More continuous data collection approaches such as airborne LiDAR (ALS) and terrestrial laser scanning (TLS) are providing ways to collect higher resolution data sets over both larger areas and less accessible locations; however, their use in management contexts has significant limitations in terms of practicality, and crucially, cost (e.g. Bangen 2014). Over the last decade, structure from motion photogrammetry (SfM) has added a new method to the geomorphologist's toolbox for topographic surveying (e.g. James and Robson 2012; Fonstad et al. 2013; Woodget and Austrums 2017). Data collection platforms for SfM can be airborne (e.g. unmanned aircraft systems (UAS)) or ground-based (e.g. telescopic poles) and the approach has been shown to be relatively simple and inexpensive compared to ALS or TLS surveys (Carrivick et al. 2016).

An increasing number of studies compare SfM and laser-based approaches for topographic surveys. Repeatedly these studies demonstrate how neither of the approaches is best for all applications (no 'one-size-fits-all') and preference for their use is dependent on specific project requirements (e.g. Wilkinson et al. 2016, Mosbrucker et al. 2017) including considerations of time, expertise and funding. This means that there is a need for examples of best practice, comparing methods for different applications, and an understanding of the advantages and disadvantages of each, so that results from different survey platforms can be merged in single projects. In this study, we

demonstrate how a camera on a (telescopic) pole, further referred to as pole aerial photograph (PAP), can significantly improve SfM data collection when the aim is to map the topography of small stream channels. This is tested through a comparison of topographic models obtained by three common survey techniques for a 100 m reach of Coledale Beck, a small upland stream in Cumbria, United Kingdom. The model results and development process from the PAP-SfM method are compared with those of the same model created by means of TLS and with those of SfM applied to photos obtained with a UAS.

## ***1.2 Tools for surveying fluvial topography: advocating SfM***

From the studies reviewing and evaluating the use of both SfM and laser-based approaches, TLS emerges as the most accurate, consistent, and reliable surveying tool (e.g. Heritage and Large 2009, Chandler and Buckley 2016, Wilkinson et al. 2016). TLS involves a ground-based laser scanner, which emits pulsed laser light and detects its reflected signal to create a dense point cloud, representing the surrounding topography. TLS is a close-range alternative to Airborne Laser Scanning (ALS), where laser point clouds are derived from an airborne platform such as an aeroplane, helicopter, or very recently a UAS (e.g. Brede et al. 2017). TLS are capable of providing high spatial resolution elevation measurements (100-10,000 points/m<sup>2</sup>; Bangen et al. 2014), with <0.001m precision and accuracy (e.g. Milan et al. 2007). However, reduced accuracies (0.1-0.3m) for bare earth surveying have been observed due to influences of surrounding vegetation (e.g. Bangen et al. 2014). Furthermore, the cost of purchase is high (c. £35,000 for a Leica Scanstation C10 and software, as used in this study) and specialist training is required to become familiar with both scanner and associated data processing software.

SfM is a relatively new photogrammetric approach originating from the field of computer vision (Lowe 2004). SfM algorithms have significantly improved traditional photogrammetric techniques, allowing 3D models to be created from a series of overlapping, convergent digital photos without the need for georeferenced camera locations and orientations or a metric camera (Rosnell and Honkavaara 2012, Westoby et al. 2012, Fonstad et al. 2013, Woodget et al. 2015, Carravick et al. 2016, Agisoft LLC 2018). These overlapping photos can be acquired using a handheld camera or a camera mounted on an elevated structure or an airborne platform. This means that SfM provides a flexible method, which can be adapted according to the requirements of a specific application, in terms of scale, temporal and spatial resolution, areal extent, features of interest (e.g. roofs, or riverbank overhangs) and viewing angle.

SfM has a number of logistical advantages, which make it attractive for environmental research and management applications. For example, (a) it permits rapid data acquisition (Verhoeven 2011, Westoby et al. 2012, Michelletti et al. 2015), (b) hardware capital costs are low (requiring a single commercial camera or smartphone) (Frankl et al. 2015, Micheletti et al. 2015, Woodget et al. 2015), (c) it achieves relative precisions of approximately 1:1000 or better (i.e. cm-scale precision over viewing distances of 10's of metres) (James and Robson 2012), (d) it offers the opportunity to generate multiple model outputs (e.g. 3D point cloud, 3D mesh, Digital Elevation Model (DEM), orthophoto) (Kaiser et al. 2014, Woodget et al. 2015) and (e) it provides flexibility regarding scaling and georeferencing (Kaiser et al. 2014). Disadvantages of the approach are that data processing can be slow given a combination of large image volumes and limited computing capacity (Westoby et al. 2012, Javernick, Brasington and Caruso 2014). SfM also experiences difficulties in modelling homogenous surfaces (e.g. sand) where image texture is lacking (Cook 2017) and in dealing with occlusions

(i.e. surface areas hidden from view by elevated elements in the landscape, such as boulders) (Micheletti et al. 2015). Furthermore, unlike ALS, dGPS and total station surveys, but in common with TLS, dense vegetation cover precludes ground surface modelling (James and Robson 2012, Javernick, Brasington and Caruso 2014, Micheletti et al. 2015, Woodget et al. 2015) and variation in light levels may reduce feature identification, restricting the opportunity of when good quality data can be acquired (Bemis et al. 2014, Micheletti, Chandler and Lane 2015). Additional concerns also exist about the ‘black box’ nature of the software (James et al. 2017) and the need for a certain level of skill and planning to acquire spatially consistent, high-quality data (Wilkinson et al. 2016). This includes the implementation of ground control points or acquisition of highly accurate dGPS locations of photo centres, to enable accurate positioning of the resulting model in absolute space.

### ***1.3 Comparing tools for surveying fluvial topography***

One of the first comparative studies looking specifically at fluvial environments was undertaken by Fonstad et al. (2013). They compared UAS SfM and ALS results with dGPS validation or ‘ground truth’ points. Mean vertical differences from the ground truth data were 0.07 m for SfM and 0.51 m for ALS and the mean difference between ALS and SfM data was 0.27 m. The reliability of these results, however, were potentially affected by discrepancies in data acquisition dates and data resolution. Smaller differences between SfM and TLS data were found by Mosbrucker et al. (2017) who estimated that change detection for each survey type differed by about 10%, where the UAS imagery had been collected from 100–600 m above ground level. Mean absolute vertical accuracies varied, but ranged from 0.02 m to 0.15 m for TLS and up to 0.37 m for the SfM data sets. They achieved significant improvements in elevation accuracy through improved camera and post-processing settings. Cook (2017)

compared results from UAS SfM with TLS data from the Daan River in Taiwan; focusing particularly on the performance of different types of UAS. The best performing SfM data showed a 0.3 m RMS error compared to the TLS data. The dominant SfM survey altitude was approximately 70 m. Hamshaw et al. (2017) found a mean error between UAS and TLS of 0.11 m in early spring ('leaf-off') conditions from flying heights around 100 m and TLS ranges of 50-300 m. Although they made no explicit comparison with laser-based tools, Javernick, Brasington and Caruso (2014) achieved vertical surface errors as low as 0.10 m from a survey altitude of c. 700 m, for a first UAS SfM survey in a complex braided river environment. Bangen et al. (2014) did not make comparisons with SfM, but found ALS and TLS uncertainties of 0.27 m and 0.81 m respectively. The ALS sensor was flown at 1300 m. The consistent message that emerges from all these recent studies is, that no single method, SfM or laser-based, is optimal in every situation. Instead, researchers should be capable of applying the most appropriate technique (or a hybrid of techniques) for a given purpose.

#### ***1.4 Pole aerial photography***

The growing popularity of SfM and developments in UAS technology is bringing greater range, stability, payload, automation, portability and affordability. However, whilst the practical operation of UAS has become significantly easier in recent years, flight and planning experience remains essential, as does knowledge of the legal and regulatory conditions within the country of operation (Cracknell 2017). For small scale, low-budget, rapid acquisition projects, such regulations can be prohibitive. A less commonly considered platform is the telescopic pole, which, with heights of 5 m or more, can provide a very effective means of data collection in many situations. Pole Aerial Photography (PAP), also referred to as Ground Photography (GP) (Glendell et al. 2017), has been used for remote sensing applications in various forms, e.g. mapping of

vegetation (Verschoren et al. 2017) and archaeological features (Verhoeven 2009). Utilising poles to create 3D models using SfM, has gained in popularity for documenting archaeological and heritage sites (Mathews and Jensen 2012, Ortiz et al. 2013). More recently, publications of geomorphological applications have started to appear. James et al. (2017) used a pole-mounted camera to collect images for measuring gully erosion, and Mathews and Jensen (2012) showed the strength of incorporating both ground and pole-based photography to provide multiple viewing angles and ranges, which increased coverage in an urban setting. The most comprehensive comparison of surveying tools including PAP has been published by Glendell et al. (2017), who assessed their suitability for erosion in upland peat soils, including gullies. Similar findings were reported by Castillo et al. (2015) and Koci et al. (2017) who successfully mapped a gully network, although their PAP findings were not compared with other tools. A summary of applications and results of PAP-based SfM further demonstrates the scarcity of studies that have employed this technique (Table 1).

[TABLE 1]

Observed advantages of the PAP platform include low cost, high mobility, ease of use (Verhoeven 2009) and higher diversity of viewing angles (Mathews and Jensen 2012). Although much wider ranges can be covered from UAVs, the closer proximity of poles to the target, allow for creation of SfM models with much greater detail (Bemis et al. 2014; Westoby et al. 2012). The greater stability of the platform may also improve image quality. In certain environments an additional advantage of PAP compared to TLS is its potential to cover a greater area in a shorter period of time, but this will depend on local morphology and the viewing angle of the instruments.

PAP clearly has a number of advantages compared to UAS and TLS data collection, though to date UAS have seen wider application in fluvial environments.



However, in scenarios where river channels are narrow and have submerged beds, we hypothesise that pole-based data collection for SfM analysis will provide a more effective way of collecting topographic data, when measured in terms of time, cost, spatial resolution, accuracy and precision. To test this hypothesis, we compare topographic models for a 100 m reach of a small upland stream obtained from three different surveying approaches:

- 1) SfM photogrammetry applied to RGB image data collected with a compact camera from a 5 m telescopic pole.
- 2) SfM photogrammetry applied to RGB image data collected with a compact camera operated from UAS.
- 3) TLS point clouds generated with a Leica ScanStation C10 from 8 scan station positions at high resolution (5 cm at 100 m range).

The details of the different methods used are described in the following section.

Meanings of acronyms and abbreviations used in the remainder of this article are defined in Table 2.

[TABLE 2]

## **2 Methods**

### ***2.1 Site and field data collection methods***

Over a period of 3 days from 6-8 July 2013, data were collected from a 100 m reach of Coledale Beck, near Braithwaite in Cumbria, UK (Figure 1). Sky conditions were bright and sunny, with light winds. This study focusses on a 50 m subset of the data (Ordnance Survey 1:5,000 map Grid Reference NY 21291 22381; 205 m AOD). The river is a

wandering 3-10 m wide, pool–riffle system and the site includes an exposed point bar and steep banks. A 13 m section of the right bank is undercut. Stream gravels are very coarse ( $D_{50} = 35$  mm) with occasional large boulders up to 0.7 m. Vegetation varies from the side slopes where acid grassland, dwarf shrub heath and bracken dominate, to the river floodplain which typically consists of bare gravel bars, grassy floodplain remnants with some isolated exposed peat. During the survey, flow was low and clear, with an average water depth of 0.14 m and a maximum water depth of 0.70 m.

The stream was selected as a rigorous test of the different methods because it displayed: (i) considerable local relief variation (i.e. channel, banks, floodplain segments and adjoining hillslopes); (ii) highly variable surface cover types (ranging from very coarse gravel to bracken vegetation); (iii) included areas of obscured topography (undercut banks); and (iv) had areas of clear standing water. In addition, the scale of enquiry was appropriate to investigations of fluvial geomorphology and stream habitat surveys (Bangen et al., 2014). Figures 2 *a* to *c* give an impression of the diversity of geomorphology found at the field site.

[FIGURE 1]

[FIGURE 2 a, b and c]

The Pole Aerial Photography (PAP) was collected using a Samsung NV24HD 10.2 megapixel consumer-grade digital RGB camera, mounted on a 5m steel and aluminium extension pole and operated using a JJC RM-E9 remote control. We took photos at approximately 5 m intervals along the channel, while walking along the edge of the riverbank in both upstream and downstream directions. The camera was directed towards the river and pointing obliquely downwards at an angle of c.  $45^\circ$ . This resulted in a total of 374 photos, with varying levels of overlap (PAP\_HQ) and a footprint of approximately  $8 \times 6$  m. We selected a sub set of 114 photos (PAP\_LQ) to assess the

impact of using a smaller number of input images on model quality. As shown in Figure 3, the aim of the PAP approach was specifically to capture detail of the channel environment and as such covers about 10% of the total area covered by the other two surveys (UAS and TLS).

[Figure 2]

We acquired RGB images from a Draganflyer X6 UAS, using a Panasonic Lumix DMC-LX3 10.1 megapixel consumer-grade digital camera (UAS). The Draganflyer X6 is a lightweight (1 kg), manually controlled, rotary-winged UAS with a 0.5 kg payload. A target flying altitude of c. 25–30 m above ground level was maintained, in combination with a focal length of 5 mm, which resulted in imagery with a pixel size of c. 0.01 m. The image size was 3648 pixels by 2736 pixels and each image footprint was approximately 25 m × 35 m. All images had c. 80% overlap, as confirmed during the manual suitability assessment of photos after data collection. We summarise the workflow of image acquisition, use of ground control and the subsequent SfM analysis steps below. Further details of each step are provided in Woodget et al. (2015).

The TLS data (TLS) were collected using a Leica ScanStation C10. This is a green wavelength (532 nm) scanner, with a 300 m range, a 360° by 270° field of view and a scan speed of up to 50,000 points per second. We positioned six, tripod-mounted, Leica HDS targets at visible locations within the area of interest, ensuring that they covered the range of elevations present at the site. We obtained high-resolution laser scans (defined as 0.05 m resolution at 100 m range) from 8 scan station positions, chosen to ensure high angles of incidence and to reduce shadowing and obscuration.

## **2.2 *PAP and UAS image data processing***

We processed the images obtained from both the UAS and PAP approaches using Agisoft Photoscan Pro (v. 0.9.1.1714 for UAS and 1.0.0.1795 for PAP). Images affected

by blur were removed prior to processing and comparable programme settings for both approaches were used where possible. Details on settings used for the UAS data can be found in Woodget et al. (2015). Details on the PAP analysis settings are attached as supplementary material. We optimised the image alignment following the input of GCP co-ordinates, and the software was used to export hyperspatial resolution orthophoto mosaics, DEMs and dense point clouds.

James and Robson (2012) showed how appropriately reducing the number of images and refining match parameters can significantly decrease reconstruction time while keeping good results. A second point cloud was therefore created for a reduced number of PAP images (approximately one third of the original dataset, see Table 3) whilst maintaining sufficient overlap to ensure successful point matching.

### **2.3 *TLS data processing***

Initial processing of the dense TLS point cloud was undertaken using Leica Cyclone 9.0 software (Leica Geosystems HDS, LLC). We removed two targets from the applied registration that produced the largest errors and used the known positions of the remaining targets and scan stations (acquired using dGPS) to georeference the merged scan to British National Grid. We performed a small amount of manual editing of the TLS point cloud to remove clearly erroneous data spikes (due to sensor saturation by sunlight) and clipped the dataset to match the extent of the UAS and PAP surveys.

As the SfM approach tends to result in more smoothed point clouds compared to higher frequency point clouds produced by the TLS, two different approaches were employed to generate a DEM from the TLS point cloud data: (1) standard interpolation in CloudCompare based on the maximum value of point falling within a given cell size (TLS\_MAX) and (2) a method developed in-house (TLS\_AVG) (Austrums, 2014). Cell values in the TLS\_MAX DEM were equal to the maximum value of the points making

up that cell in combination with default CloudCompare interpolation. Cell values in the TLS\_AVG DEM were equal to the average elevation value of points falling within each cell. A small amount of interpolation was performed to obtain elevation estimates for no-data cells in areas of sparse point density (i.e. cells that do not coincide with points in the point cloud). This was undertaken by assigning to empty cells with four or more neighbours the average cell value of these neighbouring cells. A total of 10 of these gap-filling iterations were performed. The TLS\_AVG approach results in a smoother DEM, more similar to the DEM generated from the SfM point clouds. Further details of the resulting DEMs are provided in the Results section.

#### **2.4 *Georeferencing and refraction correction***

To achieve optimal accuracies in this method comparison, all three datasets were georeferenced using the global coordinates of four permanent survey markers, obtained using a Leica GPS1200 dGPS and post-processed using RINEX data. We located the positions of TLS targets, ground control points (GCPs) and topographic survey locations relative to these permanent markers, using a Leica Builder 500 total station and a local coordinate system. We used GCPs to permit subsequent indirect georeferencing of the UAS and pole imagery: 25 GCPs to rectify the UAS data and 10 for the PAP data. The GCPs consisted of  $0.2 \times 0.2$  m black and white squares, which we positioned according to a uniform random pattern, representing the topographic variation across the site (Vericat et al. 2009). As the PAP survey was restricted to the river channel only, PAP GCPs were located only on the riverbank and riverbed, while still representing local topographic variation.

SfM has been proven successful for mapping submerged as well as terrestrial topography (e.g. Woodget et al. 2015), while TLS is predominantly used above water, due to the limitations of light absorption by water. As the visibility of submerged

topography is affected by refraction, a correction was applied to the submerged parts of the UAS and PAP models using the methods proposed for fluvial environments by Westaway, Lane and Hicks (2000, 2001) and first used in a SfM scenario by Woodget et al. (2015). Dietrich (2017) presents a more comprehensive approach to refraction correction for SfM point clouds; but given the complexity of this method and the fact that we did not expect the choice of method to have an influence on the comparative results, we applied the simpler approach of Woodget et al. (2015) to both the UAS and PAP datasets. We digitised the position of the water's edge from the orthophoto at a scale of 1:50. Next, we extracted DEM elevation values at 0.25 m intervals along this edge and used these values to generate a TIN model representing the water surface. We subtracted the underlying DEM from this surface and multiplied the resulting depth values by 1.34 (the refractive index of clear water) to produce maps of refraction corrected water depth ( $h$ ). Lastly, we obtained DEMs with refraction corrected submerged channel elevations by subtracting the difference in water depth between the non-corrected and corrected datasets from all original DEMs (UAS\_RC and PAP\_HQ\_RC).

## ***2.5 Error and performance assessment***

The quality of the topographic data produced with each approach was assessed with a set of independent elevation data, collected using a total station, across both exposed and submerged channel and floodplain surfaces. These ground validation points (GVPs) included records of water depth to the nearest centimetre and consisted of 58 points located in exposed, but vegetated areas; 86 in exposed, non-vegetated areas; and 116 points in submerged areas.

Accuracy and precision have been seen to quickly deteriorate away from ground

control points (e.g. Koci et al. 2017). For each validation measurement, distance to the nearest GCP was measured and this information was used to calculate separate accuracy assessments for data close to the GCPs (< 5 m) only. Three types of surface were mapped and used in subsequent accuracy assessments: Exposed (no vegetation), Submerged, and Exposed (vegetated). The map was created by manually outlining areas from the orthophoto at scale 1:50.

Further assessment of the performance of the three approaches was done by means of DEMs of Difference (DoD) calculations, which involves subtraction of two DEMs on a cell by cell basis. DoDs are commonly used to assess changes in topography over time. In our study however the DoDs are used to assess differences in topography as mapped by the different approaches. The DoD method, although very intuitive, does not always represent more complex topography very well (Lague, 2013), with errors occurring, where overhangs are present and in steep terrain where small lateral offsets can produce large vertical differences.

Alternatively, a direct comparison of point clouds as produced by both TLS and SfM is generally seen as more robust means to assess differences between two surfaces. It can for example use a varying surface-normal. One of the most adaptive methods is the Multiscale Model to Model Cloud Comparison (M3C2) algorithm developed by Lague et al. (2013). The M3C2 algorithm finds the best fitting normal for each point in one point cloud and calculates the distance to another point clouds by implementing a cylinder between the two clouds and calculating the distance along it. We used CloudCompare (CloudCompare 2.10.2, 2019) to do the M3C2 calculations. All comparisons used core points with 10 cm spacing, a cylinder with a 43 cm diameter, and multiscale normals with radii from 0.4 m to 2 m with a step of 0.4 m.

### 3 Results

#### 3.1 *Residual errors and resolution*

A summary of the data collected with each survey approach is listed in Table 3. The overall mean absolute error (MAE, as used in Leica Cyclone) of the TLS data was 0.009 m, and average error in the vertical dimension was 0.026 m. The resulting point cloud was exported from Cyclone as a PTS file comprising c. 165 million points with a file size of c. 9 GB. The TLS\_MAX DEM, based on maximum point values per cell, has a resolution of 0.01 m. The in-house produced TLS\_AVG DEM has a spatial resolution of 0.013 m. The pixel size of the latter approach was selected as a compromise between achieving the highest spatial resolution and minimising holes in the DEM in areas of sparser point density. In theory, the TLS\_AVG DEM could include data interpolation over distances of up to 0.13 m, but in reality, interpolation rarely extended further than 0.05 m and was not found to adversely affect subsequent analyses carried out on the data.

Both HQ and LQ PAP DEMs and orthophotos had a resolution of 0.009 m. Residual errors (standard deviation) in the  $x$  and  $y$  directions ranged from 0.021 to 0.029 m and  $z$  axis errors were precise to the cm scale (0.012 m) for both the HQ and LQ DEM. Residual errors (mean error) were generally very accurate ( $<0.002$  m) for both datasets. In the areas of interest (channel near the GCPs) the PAP\_HQ DEM appeared to have higher accuracy than PAP\_LQ DEM when compared to the GVPs (see next section), therefore further analysis was conducted on the HQ-dataset.

The UAS data accuracy, signified by the residual error (mean error), was 0.006 and 0.007 m for the  $x$  and  $y$  directions respectively, and 0.022 m in the  $z$  direction. Precision of the data, signified by the residual error (standard deviation), remained well below 0.1 m.



[TABLE 3]

### 3.2 Validation

The results for the comparison of each DEM to the ground validation data are shown in Table 4a. The results apply to the region where DEMs from all approaches overlap (Figure 3). When considering all GVPs for the whole site, UAS mean errors are lowest and PAP just out-performs TLS with slightly lower mean errors (e.g. TLS\_AVG = 0.123 m; PAP\_HQ = 0.103 m; UAS = 0.049 m). The standard deviations are again lowest for UAS data, but highest for PAP data. When looking exclusively at the GVPs in exposed (non-vegetated) areas, the error ranges amongst platforms are smallest and the lowest mean error is actually achieved by the TLS\_AVG (0.006 m). In this case both the TLS and UAS results have the highest standard deviations. Particularly for vegetated surfaces the UAS data performs better overall, with up to 100% lower mean errors (e.g. TLS\_AVG = 0.295; PAP\_HQ = 0.334; UAS = 0.177) and standard deviations (e.g. TLS\_AVG = 0.254; PAP\_HQ = 0.406; UAS = 0.191), compared to PAP and TLS.

Validation limited to data points within 5 m of GCPs shows important variation in the results (Table 4b). The area concerned consisted of an 810 m<sup>2</sup> subset of the data (Figure 3). The overall mean error for the PAP\_HQ data improves considerably (0.085 m from 0.103 m), as does the mean error for the exposed areas (0.013 m from 0.036 m). This indicates that the distribution/number of GCPs has an impact on the PAP data quality. A positive (0.235) significant ( $\alpha < 0.01$ ) correlation ( $n = 260$ ) was found between mean error and distance from GCPs for the PAP\_HQ DEM.

The higher mean errors found for both TLS\_AVG and TLS\_MAX when considering the whole site were contrary to our expectations. Because of these results, in combination with observations from the DEM of difference visual displays (presented in

section 3.3), we considered the possibility that an offset in the TLS data had occurred. To test this hypothesis, both the TLS DEMs and the UAS DEM were realigned with the PAP\_HQ data, as the latter appeared to be the most accurate data set (0.036 m, assuming exposed, unvegetated control points were most reliable, according to experiences documented in the literature). Realignment was undertaken based on a set of manually identified tie points. The results of a comparison of the realigned data with the ground validation points are included in Table 4c (using GEOREF suffix). After realignment both the mean error and standard deviation of the TLS data increases by variable amounts. The same is observed for the UAS errors, apart from the exposed surfaces, where the UAS mean error is as low as 0.001 m. These findings imply that the realignment did not necessarily improve the results. Hence an alternative explanation may be that the poorer overall performance (i.e. at all GVPs) of TLS is a reflection of its weak performance in both submerged and vegetated areas, in contrast to its superior performance in exposed areas.

[TABLE4]

Figure 4 shows the spatial distribution of differences between the DEM values and the ground validation data for each approach. The largest positive and negative errors (>0.5 m) are typically found on the vegetated surfaces away from the river and along the river's edge due to steep and overhanging banks and bank vegetation.

[FIGURE 4]

### ***3.3 DEMs of difference and cloud comparisons***

Figure 5 shows the DEM of difference (DoD) between the TLS\_AVG DEM and the UAS data. The majority of the data indicates that the TLS\_AVG DEM sits above the UAS DEM, with large parts of the densely vegetated banks and hillslopes adjacent to

the banks, showing greater than 0.05 m elevation difference. Along the exposed gravel bars the TLS DEM is typically 0.02-0.05 m higher than the UAS DEM. In contrast, the TLS DEM is lower than the UAS DEM along the edges of steep, overhanging banks and along other key breaks of slope in vegetated areas.

The inset image in Figure 5 appears to show a shadow effect around larger boulders. Compared to the UAS DEM, the south-westerly sides show higher elevation in the TLS DEM and the north-easterly sides show lower elevation in the TLS DEM. As before, this suggests there is either an offset in the two datasets or it reflects the differential measurement capabilities of terrestrial oblique versus airborne sensor platforms. Figure 5 also shows that the DEM created from the Coledale Beck UAS data is affected by doming. Doming in the data is thought to occur due to the inaccurate correction of radial lens distortion within the SfM software and when image acquisition is predominantly at nadir (James and Robson 2014). The effect is particularly visible along the exposed gravel bars where, near the edges of the DoD, the TLS DEM appears to have much higher elevation values than the UAS DEM, compared to the centre. The spatial pattern of over and underestimation in vegetated and bank areas is similar when a DoD is created for the PAP\_HQ DEM and the TLS DEMs (for both TLS\_AVG and TLS\_MAX, but only TLS\_AVG shown in Figure 7 and 8), however extremes of the model don't display the same deformation due to doming. Some notable underestimation of TLS\_AVG compared to PAP\_HQ occurs at the western edge of the DoD and to a lesser extent on the eastern edge. This pattern does not show the image-wide gradual change resulting from the doming effect, as highest differences seem to be much more restricted to the edge of the PAP model only, which is most likely due to the reduced number of photos covering these areas. Similar boundary issues were not found

for the UAS data as this covered a considerably larger area. . The effect is also visible from the relatively high errors at the GVPs in these areas in Figure 4a.

Quantitative results of the DoD comparisons (Table 5) show mixed results, with the TLS data compared to the PAP\_HQ data resulting in the greatest mean difference for exposed areas ( $>0.042$  m), while UAS compared to the PAP HQ show the greatest mean difference for vegetated surfaces (0.140 m). The realigned image data compared to the original data gives the impression of an improved image overlay with less ‘shading’ effects around the boulders (Figures 6 and 8). However, the quantitative assessment does not clearly confirm this, which could be the result of other mismatches being introduced elsewhere in the images due to the realignment, which further indicates that misalignment is not the cause of TLS underperformance. Highest standard deviations consistently occur in the vegetated parts of all DoDs and overall the PAP\_HQ data compares well with both the TLS and UAS.

[FIGURE 5]

[FIGURE 6]

[FIGURE 7]

[FIGURE 8]

[TABLE 5]

The results of the M3C2 cloud-to-cloud distance assessment for the exposed and vegetated areas are listed in Table 6. The results seem similar to the DoD assessments, with the greatest M3C2 distances found for TLS and PAP\_HQ in exposed areas (0.061m) and for UAS and PAP HQ on vegetated surfaces (-0.104m). However, for the latter comparison the PAP\_HQ cloud has the highest values, while in the DoD comparison the UAS surface is the highest. So, although the magnitude of differences

found with both methods is quite similar, there are some considerable, though not obviously consistent, differences (indicated with thick cell borders).

## **4 Discussion**

### **4.1 Accuracy comparison**

The comparison of DEM elevation values with the independent topographic validation data suggests that the accuracy and precision of the UAS and PAP DEMs are better than that of the TLS DEM throughout the study area (Table 4a). Overall TLS mean errors (0.123-0.135 m) are approximately 150% higher than the UAS error and 20% higher than the PAP errors (ranging from 0.031-0.103 m). The standard deviation is approximately 25% higher for PAP DEMs, but 45% lower for UAS DEMs.

Considerable variations in error values occur when we differentiate the results by surface type. On exposed surfaces the lowest mean error (0.006 m) is achieved by the TLS\_AVG. Figure 4c shows the spatial distribution of TLS DEM errors. This confirms that TLS over-predicts elevation particularly in the vegetated and submerged areas, but less so in the exposed areas, though more under-predictions are observed here as well. It also further visualises the TLS under-predictions taking place on the right riverbank near a section that was recorded as over-hanging, which may partly explain the negative errors. Variation in error is very small between UAS and PAP results, but UAS clearly performs better under vegetated conditions.

### **4.2 DoDs vs. M3C2**

The difference results obtained by the DoD and M3C2 comparison methods are mostly similar for the different surface types. However, a closer look at the distribution on of the greatest differences does show some variation between the two approaches. The M3C2 method shows consistently highest differences in the more densely vegetated

southeast corners of the field site, though the effect is greatest for comparisons including the pole point cloud. This is therefore most likely a combination of the rough vegetation surface as well as the sparser coverage of photos from the pole approach in this area. The TLS and pole DoDs show specifically high differences along the river bank (Figure 7), due to the way these survey methods record the steep and overhanging bank edge, by averaging points from the top of the bank and those located on steep bank sides or under overhangs. The cloud-to-cloud method on the other hand shows the smallest distances in such locations for the TLS and pole comparison. Relatively large distances are instead found for the TLS and UAS comparison, where the UAS point cloud does not extend underneath the overhanging bank or cover the steep bank sides. As the steep/overhanging bank coincides with the boundary between the exposed and vegetated areas, its effect will be included equally in the distance estimates of both types of environments.

Contrary to studies that look at topographic change over time, we merely used the DoDs to assess relative differences between the three survey methods and their spatial patterns. Both the DoDs and the cloud-to-cloud comparisons in this case provide specific insight in the performance of the three survey methods. For example, the DoDs give a better impression of the spatial extent bank overhangs, while the cloud-to-cloud comparisons allows confirmation of the actual form of such complex morphology. However, in the future more specifically targeted ground validation data will need to be collected for the validation of the full 3D morphological assessment.

### **4.3 *Surface types***

The poorer performance of TLS and mixed performance of PAP (PAP\_LQ versus PAP\_HQ), compared to the UAS approaches under vegetated conditions, is mostly due to the oblique viewing angle of the TLS and PAP platforms. This makes them more

likely to sense the upper elevations of plants in areas with dense vegetation, compared to methods that have a viewing angle closer to nadir, like the UAS approach. Consequently, TLS is more likely to over-predict elevation under such conditions, as it produces a Digital Surface Model (DSM) rather than a Digital Terrain Model (DTM). In contrast, under-estimations are thought to have occurred where the oblique viewing angle allowed measurements to be taken underneath over hanging banks, while the independent validation data was taken from the top of the banks. In areas with little or no vegetation cover the TLS survey outperforms both other approaches. More continuous data was collected and the TLS DEM mean error is clearly lower than in other parts of the scene and even slightly better than those of the UAS and PAP DEMs. Similar findings of different systematic errors for different surface types have been reported for other SfM and TLS based studies (e.g. Hamshaw et al. 2017, Bangen et al. 2014).

Besides influencing the accuracy of the surveying results, vegetation can also influence site access. Dense riparian vegetation will hinder both the Pole-SfM and TLS data collection. On the one hand this means that the UAS approach will have an advantage where lower canopy vegetation impairs access. However, a pole/hand-held perspective can be used around higher canopy bank vegetation and therefore access channel stretches that will be very difficult to view from or navigate with a UAS (Hamshaw et al. 2017).

#### **4.4 Refraction**

The overestimation of the TLS elevations in the submerged parts of the DEM are likely to result from the oblique viewing angle of the scanner (with additional errors possibly resulting from full/partial absorption of laser light by the water and subsequent

interpolation). This results in greater refraction angles in these areas, which results in over-prediction of the channel bed elevations. This effect is also observed in the UAS and PAP data. While the UAS and PAP submerged data were corrected for refraction, this process was not attempted for the TLS data. Some successful attempts at refraction correction for TLS data have been documented (e.g. Smith, Vericat and Gibbins 2012, Smith and Vericat 2014), but they were applied at a coarser resolution (Smith and Vericat 2014), and in this project time and software constraints prevented further correction attempts. In this study TLS does not produce any returns at water depths  $> c. 0.3$  m, which results in gaps in the DEM for large parts of the submerged stream channel. The UAS and PAP data does cover most of the submerged stream channel, but the refraction correction approaches have only been shown to work in clear water streams to depths of  $c. 0.7$  m (Woodget et al., 2015). This corresponds with the maximum depths achieved with other surveying methods.

There is some potential to make the refraction correction process more efficient and accurate in cases, where Near Infrared (NIR) photos can be collected simultaneously. Limited data collection with a Near Infrared sensitive camera during this project indicated that ‘water’s edge’ detection can be achieved more accurately and efficiently through automatic land/water classification of an orthophoto derived from and additional set of NIR photos.

When submerged topography is an essential component of the 3D model that needs to be produced, it is essential to collect data under clear sky conditions. Cloud cover creates diffuse lighting conditions which make it much more difficult/impossible to see/photograph through the water surface. Sun glint can affect visibility under sunny conditions, but it is a very localized effect which can be masked out, as long as further



unobscured images from different viewing angles are available. TLS should not be affected by sky cover conditions.

#### **4.5 *Geometry of ground control***

As the PAP SfM approach predominantly focusses on the stream topography (with a limited capture of adjacent areas), photos are taken along an approximately linear path in the landscape. GCPs were positioned along the stream in a similar linear fashion, which is not an optimal pattern (Woodget et al. 2015). Consequently, accuracy and precision quickly deteriorate away from the centre of the PAP SfM model. Reduced photo coverage and potentially a doming effect will also contribute to this result.

Planning of the acquisition geometry is an important aspect of the SfM process and needs to be done well to obtain the best results emphasizing GCP quality over quantity (James and Robson, 2012, Javernick, Brasington and Caruso 2014, Stumpf et al. 2015). Castillo et al. (2015) for example, found a mean error of 0.069 m at the ground control points, mostly due to model deformations emanating from the linear geometry of the gully they observed and residual errors in camera calibration. Our data collection approach at Coledale Beck was similar to that suggested by Koci (2017) for dryland gullies and very similar resolution and vertical errors were observed.

Using a Direct Georeferencing approach, as presented by Carbonneau and Dietrich (2017), however, GCPs may become unnecessary, while producing results without doming effects. At this point the results are not yet of survey grade quality, but higher-grade GPS, amongst other factors, are set to further improve these results. An important note made by the authors is however that SfM is photogrammetry and therefore requires traditional knowledge and essential analysis steps from this field such

as accurate camera calibration. Their findings also confirmed earlier observations that SfM precision is inherently limited to a scale of 1:1000.

#### **4.6 Data interpolation/post processing**

The processes by which Leica Cyclone (TLS) and AgiSoft PhotoScan generate 3D point clouds (and DEMs) are significantly different and therefore complicates direct comparisons. The TLS software creates points at a position regardless of surrounding points, whereas PhotoScan interpolates between key features. This means that PhotoScan automatically reduces noise. Additional post processing of the TLS point cloud may be needed depending on the given application (for example point clouds can be classified by surface roughness and elevation statistics). This can be considered an advantage and a disadvantage depending on the application (time vs versatility vs expertise). TLS\_MAX showed consistently larger residual and DoD errors (between 10% and 50%) compared to TLS\_AVG (e.g. 0.042 vs. 0.054 m error in exposed areas) for the TLS – PAP\_HQ DoD (Table 5), which potentially explains the slightly larger errors found near the riverbanks in the DoDs (see close-ups in Figure 9), as the abrupt elevation changes at the river bank will be misrepresented more easily at the point cloud interpolation stage when maximum point values are used instead of average values. This highlights the importance of clear documentation of post processing techniques.

[FIGURE 9]

#### **4.7 TLS performance**

Since TLS measurements are frequently used to validate topographic models derived from UAS imagery (e.g. Westoby et al. 2012), we initially expected higher whole scene accuracy and precision values from the TLS. However, results demonstrate better whole scene performance by the PAP-SfM and UAS-SfM tools. Visual evaluation of DoD

results suggested that there may be a systematic offset in the TLS data. Manual realignment of both the TLS and UAS data did not however improve the comparison with GVPs for the TLS data and, despite apparent visual improvement in the DoD displays (Figures 6 and 8), the quantitative results did not notably improve. Results of the realignment for UAS data were ambiguous with lower GVP errors for exposed areas, but increased errors overall. The impact of vegetation and submerged channel bed topography are likely to have had a significant influence on TLS performance at this site. The small error ranges are overruled by natural variation in the data (e.g. due to presence/absence of vegetation).

#### **4.8 Application potential of PAP**

Considering the overall precision and accuracy, the UAS and PAP DEMs showed the best overall results for this particular site, which has heavy lower canopy vegetation covers. An additional advantage of the UAS and PAP DEM data is that they contain fewer gaps compared to the TLS data. However, where a view of the terrain is not impacted by vegetation or the presence of water, TLS still provides the most accurate and highest resolution DEMs. The main difference between the UAS and PAP approaches is the greater distance from which the target is photographed by UAS, which results in a significantly larger ground sampling distance (GSD) compared to the TLS and PAP method. Furthermore, these results need to be considered in the context of data acquisition time and cost. At the time of writing, TLS systems remain significantly more expensive to purchase (c. £35,000 for a Leica ScanStation C10 + software, Leica Geosystems Ltd 2018) than a UAS set-up equivalent to the one used here (< £1000 for a DJI F550 UAS including camera, DJI 2018). The PAP set-up is however only as costly as the camera you decide to use. In the current example, the collection of TLS data was most efficient (854 m<sup>2</sup>/hour), followed closely by the UAS

approach. The PAP data collection was only half as efficient (430 m<sup>2</sup>/hour). As more sophisticated UAS models have come to market since this study was undertaken, higher cost efficiency can probably be achieved for the UAS approach, though this factor remains weather dependent. For short and narrow river reaches, PAP seems the most suitable topographic surveying approach; it however becomes impractical as reach lengths and channel sizes increase. To some extent, use of low-flying rotary winged UAS can overcome this constraint, as they will be able to cover longer reaches in a shorter time. Issues with overhanging vegetation will remain and line-of-sight will be far less for low-flying vehicles.

Keeping in mind the variety of nadir and oblique images obtained from UAS and PAP platforms, a combination of both data sets was briefly considered as a possible way to further improve our results. However, several attempts of running the SfM analysis on the combined data sets did not produce credible results. Our attempts included implementation of multiple manual tie points to facilitate connections between the images representing different scales. We conclude from this attempt that combining two sets of multi-scale data to obtain better models results is certainly not a straightforward process that can simply be undertaken by average software users.

#### **4.9 *Future prospects***

Observations by Smith and Vericat (2015) suggest that for detailed information requirements (e.g. soil erosion estimates) UAS observation ranges of around 10 m should be used. These are quite low flying elevations for a UAS, requiring an experienced pilot. In such situations a pole-based platform may be preferable. Following improvement in 3D point cloud analysis workflows, low range and diverse viewing angle approaches (such as a pole) will also have greater appeal as they have the potential to capture more complex topography, such as overhanging banks (Figure 10).

With the rapid development of UAS technology the PAP approach may be less desirable due to the challenge of using a long pole in awkward terrain. Although UAS battery life, construction fragility and/or weight remain constraining factors. In addition to this it is in some situations simply impossible to legally collect image data using a UAS. For example, in the UK a UAS should not be flown within 150m of any congested area (Simic Milas, Cracknell and Warner 2018). This includes most urban environments, which therefore severely limits the use of UAS-s for data collection on urban rivers. Consequently, for certain application scenarios a simple pole-based solution forms an important part of a geomorphologist's toolbox.

Overall, the PAP approach can compete with the UAS and TLS approaches, if the focus is on in channel topography. This reflects a shorter platform to feature-of-interest range (increasing resolution) and the inclusion of additional camera angles. This confirms the findings of Glendell et al. (2017), who found the advantage of PAP for measuring peat in upland environments to be at the plot scale, including the mapping of gully erosion. Although specific topographic survey methods may result in greater spatial coverage (e.g. ALS), precision (e.g. total station), or resolution (e.g. TLS), the cost and legality of acquiring data with such methods may prohibit their use in many applications. While spatial extent, precision, and resolution all factor into overall survey quality, the effort, efficiency, and cost of collecting topographic data are nearly always necessary considerations (Bangen et al. 2014).

[FIGURE 10]

## **5 Conclusion**

This study demonstrates that for mapping channel topography of small rivers, a surveying approach using PAP in combination with SfM, produces results comparable with UAS and TLS surveying tools. The different approaches all produce results of

sufficient quality to enhance understanding of fluvial forms and processes, with DEM/point cloud resolutions around 0.01 m for the close-range methods (TLS and PAP) and 0.02 m for the longer range UAS method. Residual errors of the topographic models show that the highest accuracy and precision was achieved by collecting an extensive set of photos, using pole aerial photography (PAP\_HQ) in combination with SfM data analysis, producing errors between 0.103 and 0.036 m. Important additional advantages of this method are the high resolution (compared to UAS) and its better ability to model submerged environments (compared to TLS). Perhaps most importantly for professional DEM requirements, it is an extremely cost-effective and easy to use approach. The only downside is the relatively low data collection efficiency, however the difference is not excessive and can easily be mitigated with additional field time or staff resource, as equipment is inexpensive, and limited specialist skills are required (during the data collection stage). Accuracy assessment (via total station) resulted in the expected sub-centimetre precision in the exposed areas for the TLS approach (e.g. Westoby et al. 2012), but results deteriorated in more complex submerged and vegetated environments, while PAP errors were overall slightly lower compared to other methods. With better resolution, lightweight cameras, as well as lighter weight poles becoming available, the PAP approach provides a quick and easy survey solution, which meets the increasing demand for very/ultra-high resolution image data. Unless catchment scale coverage is needed (e.g. Smith and Vericat, 2015) the pole aerial photography should be seriously considered as a useful method for obtaining topographic models from small streams. It provides a quick, low cost method, which can be integrated easily in to fluvial geomorphological reach-based assessment and stream habitat surveys. UAS and TLS approaches are more suitable where direct access to the area of interest is not possible or too dangerous. Therefore, knowing the relative

merits of these various approaches and the respective errors remains important when selecting an appropriate survey method.

## 6 Acknowledgements

This project was supported with a grant of the British Society for Geomorphology (to AW), a University of Worcester Vacation Research Assistantship (to FV), and a Bath Spa University research grant (to RJ). Additional fieldwork and equipment support was also provided by the University of Worcester, Bath Spa University (including Milo Creasey and Carl Greenman), and Durham University. We also thank Robbie Austrums for the point cloud interpolation code.

## 7 References

- Bangen, S. G., J. M. Wheaton, N. Bouwes, B. Bouwes, and C. Jordan. 2014. "A Methodological Intercomparison of Topographic Survey Techniques for Characterizing Wadeable Streams and Rivers." *Geomorphology* 206: 343–361. doi:[10.1016/j.geomorph.2013.10.010](https://doi.org/10.1016/j.geomorph.2013.10.010).
- Bemis, S. P., S. Micklethwaite, D. Turner, M. R. James, S. Akciz, S. T. Thiele, and H. A. Bangash. 2014. "Ground-Based and UAV-Based Photogrammetry: A Multi-Scale, High-Resolution Mapping Tool for Structural Geology and Paleoseismology." *Journal of Structural Geology* 69 (Part A): 163–178. doi:[10.1016/j.jsg.2014.10.007](https://doi.org/10.1016/j.jsg.2014.10.007).
- Brede, B., A. Lau, H. M. Bartholomeus, and L. Kooistra. 2017. Comparing RIEGL RiCOPTER UAV LiDAR Derived Canopy Height and DBH with Terrestrial LiDAR. *Sensors* 17 (10): 2371. doi:10.3390/s17102371.
- Carbonneau, P. E. and J.T. Dietrich. 2017. "Cost-Effective Non-Metric Photogrammetry from Consumer-Grade SUAS: Implications for Direct Georeferencing of Structure from Motion Photogrammetry." *Earth Surface Processes and Landforms* 42 (3): 473–486. doi:[10.1002/esp.4012](https://doi.org/10.1002/esp.4012).
- Castillo, C., M. R. James, M. D. Redel-Macías, R. Pérez, and J.A. Gómez. 2015. "SF3M Software: 3-D Photo-Reconstruction for Non-Expert Users and Its Application to a Gully Network." *Soil* 1 (2): 583–594. doi:[10.5194/soil-1-583-2015](https://doi.org/10.5194/soil-1-583-2015).
- Chandler, J. H. and S. Buckley. 2016. "Structure from motion. (SFM) photogrammetry vs terrestrial laser scanning." In *Geoscience Handbook 2016*, edited by Carpenter, M.B. and Keane, C.M., AGI Data Sheets, 5th ed.

- Cook, K. L. 2017. "An Evaluation of the Effectiveness of Low-Cost UAVs and Structure from Motion for Geomorphic Change Detection." *Geomorphology* 278: 195–208. doi:[10.1016/j.geomorph.2016.11.009](https://doi.org/10.1016/j.geomorph.2016.11.009).
- Cracknell, A. 2017. "UAVs: regulations and law enforcement" *International Journal of Remote Sensing* 38 (8-10): 3054-3067. doi:10.1080/01431161.2017.1302115.
- Dietrich, J. T. 2017. "Bathymetric Structure-from-Motion: Extracting Shallow Stream Bathymetry from Multi-View Stereo Photogrammetry." *Earth Surface Processes and Landforms* 42 (2): 355–364. doi:[10.1002/esp.4060](https://doi.org/10.1002/esp.4060).
- Fonstad, M.A., J. T. Dietrich, B. C. Courville, J. L. Jensen, and P. E. Carbonneau. 2013. "Topographic Structure from Motion: A New Development in Photogrammetric Measurement." *Earth Surface Processes and Landforms* 38 (4): 421–430. doi:[10.1002/esp.3366](https://doi.org/10.1002/esp.3366).
- Frankl, A., C. Stal, A. Abraha, J. Nyssen, D. Rieke-Zapp, A. De Wulf, and J. Poesen. 2015. "Detailed Recording of Gully Morphology in 3D through Image-Based Modelling." *Catena* 127: 92–101. doi:[10.1016/j.catena.2014.12.016](https://doi.org/10.1016/j.catena.2014.12.016).
- Glendell, M., G. McShane, L. Farrow, M. R. James, J. Quinton, K. Anderson, M. Evans, et al. 2017. "Testing the Utility of Structure-from-Motion Photogrammetry Reconstructions Using Small Unmanned Aerial Vehicles and Ground Photography to Estimate the Extent of Upland Soil Erosion." *Earth Surface Processes and Landforms* 42 (12): 1860–1871. doi:[10.1002/esp.4142](https://doi.org/10.1002/esp.4142).
- Hamshaw, S. D., T. Bryce, D. M. Rizzo, J. O'Neil-Dunne, J. Frolik, and M.M. Dewoolkar. 2017. "Quantifying Streambank Movement and Topography Using Unmanned Aircraft System Photogrammetry with Comparison to Terrestrial Laser Scanning." *River Research and Applications* 33 (8): 1354–1367. doi:[10.1002/rra.3183](https://doi.org/10.1002/rra.3183).
- Heritage, G., and A. Large. 2009. *Laser Scanning for the Environment Sciences*. London: John Wiley & Sons. doi:10.1002/9781444311952.
- James, M. R. and S. Robson. 2012. "Straightforward Reconstruction of 3D Surfaces and Topography with a Camera: Accuracy and Geoscience Application." *Journal of Geophysical Research-Earth Surface* 117: F03017. doi:[10.1029/2011JF002289](https://doi.org/10.1029/2011JF002289).
- James, M. and S. Robson. 2014. "Mitigating systematic error in topographic models derived from UAV and ground-based image networks." *Earth Surface Processes and Landforms* 39: 1413-1420. doi:10.1002/esp.3609.
- James, M.R., S. Robson, S. d'Oleire-Oltmanns, and U. Niethammer. 2017. "Optimising UAV topographic surveys processed with structure-from-motion: Ground control quality, quantity and bundle adjustment." *Geomorphology*. 280: 51–66. doi:10.1016/j.geomorph.2016.11.021.
- Javernick, L., Brasington, J., and B. Caruso. 2014. "Modeling the topography of shallow braided rivers using Structure-from-Motion photogrammetry." *Geomorphology* 213: 166-182. doi: 10.1016/j.geomorph.2014.01.006.
- Kaiser, A., F. Neugirg, G. Rock, C. Müller, F. Haas, J. Ries, and J. Schmidt. 2014. "Small-scale surface reconstruction and volume calculation of soil erosion in complex Moroccan gully morphology using structure from motion." *Remote Sensing*. 6: 7050-7080. doi:10.3390/rs6087050.
- Koci, J., B. Jarihani, J. X. Leon, R. C. Sidle, S. N. Wilkinson, and R. Bartley. 2017. "Assessment of UAV and Ground-Based Structure from Motion with Multi-View Stereo Photogrammetry in a Gullied Savanna Catchment." *Isprs International Journal of Geo-Information* 6 (11): 328. doi:[10.3390/ijgi6110328](https://doi.org/10.3390/ijgi6110328).
- Lowe, D. G. 2004. "Distinctive image features from scale-invariant keypoints." *International Journal of Computer Vision*. 60: 91–110. doi:10.1023/B:VISI.0000029664.99615.94.



- Mathews, A. J. and Jensen, J. L. R. 2012. "Three-Dimensional Building Modeling Using Structure from Motion: Improving Model Results with Telescopic Pole Aerial Photography. In *Proceedings of 35th Applied Geography Conference*, Minneapolis, MN, USA, 10–12 October 2012: 98–107.
- Micheletti, N., J. H. Chandler, and S. N. Lane. 2015. "Investigating the Geomorphological Potential of Freely Available and Accessible Structure-from-Motion Photogrammetry Using a Smartphone." *Earth Surface Processes and Landforms* 40 (4): 473–486. doi:[10.1002/esp.3648](https://doi.org/10.1002/esp.3648).
- Milan, D. J., G. Heritage, and D. Hetherington. 2007. "Application of a 3D laser scanner in the assessment of erosion and deposition volumes and channel change in a proglacial River". *Earth Surface Processes and Landforms* 32 (11): 1657–1674. doi:10.1002/esp.1592.
- Mosbrucker, A.R., J. J. Major, K. R. Spicer, and J. Pitlick. 2017. "Camera system considerations for geomorphic applications of SfM photogrammetry". *Earth Surface Processes and Landforms* 42 (6): 969-986. doi:10.1002/esp.4066.
- Ortiz, J., M. L. Gil, S. Martínez, T. Rego, G. Meijide. 2013. "Three-dimensional modelling of archaeological sites using close-range automatic correlation photogrammetry and low-altitude imagery." *Archaeological Prospection* 20(3): 205-217. doi:10.1002/arp.1457.
- Prosdoci, M., S. Calligaro, G. Sofia, G. Dalla Fontana, and P. Tarolli. 2015. "Bank erosion in agricultural drainage networks: new challenges from structure-from-motion photogrammetry for post-event analysis." *Earth Surface Processes and Landforms* 40: 1891–1906. doi:10.1002/esp.3767.
- Rosnell, T., and E. Honkavaara. 2012. "Point Cloud Generation from Aerial Image Data Acquired by a Quadcopter Type Micro Unmanned Aerial Vehicle and a Digital Still Camera." *Sensors* 12 (1): 453–480. doi:[10.3390/s120100453](https://doi.org/10.3390/s120100453).
- Simic Milas, A., A. P. Cracknell and T. A. Warner. 2018 "Drones – the third generation source of remote sensing data." *International Journal of Remote Sensing* 39 (21): 7125-7137. doi:[10.1080/01431161.2018.1523832](https://doi.org/10.1080/01431161.2018.1523832).
- Smith, M. W., J. L. Carrivick, J. Hooke, and M. J. Kirkby. 2014. "Reconstructing flash flood magnitudes using 'Structure-from-Motion': A rapid assessment tool." *Journal of Hydrology* 519 (Part B): 1914-1927. doi:10.1016/j.jhydrol.2014.09.078.
- Smith, M. W., and D. Vericat. 2014. "Evaluating Shallow-Water Bathymetry from Through-Water Terrestrial Laser Scanning Under a Range of Hydraulic and Physical Water Quality Conditions." *River Research and Applications* 30 (7): 905–924. doi:[10.1002/rra.2687](https://doi.org/10.1002/rra.2687).
- Smith, M. W., and D. Vericat. 2015. "From experimental plots to experimental landscapes: topography, erosion and deposition in sub-humid badlands from Structure-from-Motion photogrammetry" *Earth Surface Processes and Landforms* 40 (12): 1656-1671. doi:10.1002/esp.3747.
- Smith, M., D. Vericat, and C. Gibbins. 2012. "Through-Water Terrestrial Laser Scanning of Gravel Beds at the Patch Scale." *Earth Surface Processes and Landforms* 37 (4): 411–421. doi:[10.1002/esp.2254](https://doi.org/10.1002/esp.2254).
- Stumpf, A., J. –P. Malet, P. Allemand, M. Pierrot-Deseilligny, and G. Skupinski. 2015. "Ground-Based Multi-View Photogrammetry for the Monitoring of Landslide Deformation and Erosion." *Geomorphology* 231: 130–145. doi:[10.1016/j.geomorph.2014.10.039](https://doi.org/10.1016/j.geomorph.2014.10.039).
- Verhoeven, G. J. J. 2009. "Providing an archaeological bird's-eye view—an overall picture of ground-based means to execute low-altitude aerial photography (LAAP) in Archaeology." *Archaeological Prospection* 16 (4): 233-249. doi:10.1002/arp.354.

- Verhoeven, G. J. J. 2011. "Taking computer vision aloft—archaeological three-dimensional reconstructions from aerial photographs with photoscan." *Archaeological Prospection* 18 (1): 67-73. doi:10.1002/arp.399.
- Verschoren, V., J. Schoelynck, K. Buis, F. Visser, P. Meire, and S. Temmerman. 2017. "Mapping the Spatio-Temporal Distribution of Key Vegetation Cover Properties in Lowland River Reaches, Using Digital Photography." *Environmental Monitoring and Assessment* 189 (6): 294. doi:[10.1007/s10661-017-6004-5](https://doi.org/10.1007/s10661-017-6004-5).
- Westaway, R. M., S. N. Lane, and D. M. Hicks. 2000. "The Development of an Automated Correction Procedure for Digital Photogrammetry for the Study of Wide, Shallow, Gravel-Bed Rivers." *Earth Surface Processes and Landforms* 25 (2): 209–226. doi:10.1002/(SICI)1096-9837(200002)25:2<209::AID-ESP84>3.0.CO;2-Z
- Westaway, R. M., S. N. Lane, and D. M. Hicks. 2001. "Remote Sensing of Clear-Water, Shallow, Gravel-Bed Rivers Using Digital Photogrammetry." *Photogrammetric Engineering and Remote Sensing* 67 (11): 1271–1281.
- Westoby, M. J., J. Brasington, N. F. Glasser, M. J. Hambrey, and J. M. Reynolds. 2012. "'Structure-from-Motion' Photogrammetry: A Low-Cost, Effective Tool for Geoscience Applications." *Geomorphology* 179: 300–314. doi:[10.1016/j.geomorph.2012.08.021](https://doi.org/10.1016/j.geomorph.2012.08.021).
- Wilkinson, M. W., R. Jones, C. E. Woods, S. Gilment, K. McCaffrey, S. Kokkalas, and J. Long. 2016. "A Comparison of Terrestrial Laser Scanning and Structure-from-Motion Photogrammetry as Methods for Digital Outcrop Acquisition." *Geosphere* 12 (6): 1865-1880. doi:[10.1130/GES01342.1](https://doi.org/10.1130/GES01342.1).
- Woodget, A. S., and R. Austrums. 2017. "Subaerial gravel size measurement using topographic data derived from a UAV-SfM approach." *Earth Surface Processes and Landforms* 42 (9): 1434-1443. doi:10.1002/esp.4139
- Woodget, A. S., P. E. Carbonneau, F. Visser, and I. P. Maddock. 2015. "Quantifying Submerged Fluvial Topography Using Hyperspatial Resolution UAS Imagery and Structure from Motion Photogrammetry." *Earth Surface Processes and Landforms* 40 (1): 47–64. doi:[10.1002/esp.3613](https://doi.org/10.1002/esp.3613).
- Young, E. J. 2012. "dGPS." In *Geomorphological Techniques (Online Edition)*, edited by S. J. Cook, L. E. Clarke, and J. M. Nield. British Society for Geomorphology; London, UK. ISSN: 2047-0371.

## 8 Tables

Table 1. Overview of results from SfM studies using pole/handheld image data collection techniques, including, where known, standard deviation (SD) and root mean square error (RMSE) as measures of accuracy.

Platform	Height (m)	Target/Application	Accuracy (m)	Source
Handheld	Eye-level?	Cliff face	SD: 0.013–0.070 RMSE 0.036	James and Robson 2012
Handheld	Eye-level?	Geoscience applications	SD (z): 0.100 (no vegetation) DEM-TLS	Westoby et al. 2012

Handheld	Eye-level?	Geology	Unknown	Bemis et al. 2014
Handheld	Eye-level?	Flash flood magnitude	SD: 0.420 - 0.126 RMSE: 0.135 - 0.489	Smith et al. 2014
Handheld	Eye-level?	Gully morphology	SD: 0.011 - 0.190 RMSE (z): 0.148-0.155	Frankl et al. 2015
Handheld	Eye-level?	Riverbank (and alluvial fan)	Best median error: 0.0032 Best RMSE: .0168	Micheletti, Chandler and Lane 2015
Handheld	Eye-level?	Bank erosion	SD: 0.040 - 0.042 RMSE: 0.048 - 0.048	Prosdocimi et al. 2015
Pole	6	Gully morphology	Ground control point error 0.069	Castillo et al. 2017
Pole	5	Plot scale erosion features	RMSE 0.011 – 0.291	Glendell et al. 2017
Handheld	1.5	Gully morphology	RMSE 0.030 – 0.039	Koci et al. 2017

Table 2. Abbreviations and acronyms commonly used in this paper.

Acronym/ abbreviation	Description	Acronym/ abbreviation	Description
ALS	Airborne Laser Scanner	PAP_LQ	DEM from Low Quality Pole Aerial Photography data set (114 photos)
DEM	Digital Elevation Model	PAP_HQ_RC	DEM from High Quality Pole Aerial Photography data corrected for refraction
DoD	DEM of Difference	RGB	RGB colour model
dGPS	(differential) Global Positioning System	SfM	Structure from Motion
GEOREF	Suffix used for manually realigned DEMs	TLS	Terrestrial Laser Scanner
GCPs	Ground Control Points	TLS_MAX	DEM from Terrestrial Laser Scanner point cloud with standard (CloudCompare) interpolation, based on maximum point value.
GVPs	Ground Validation Points	TLS_AVG	DEM from Terrestrial Laser Scanner point cloud with custom interpolation, based on average point value
M3C2	Multiscale Model to Model Cloud Comparison	UAS	Unmanned Aerial System/drone

PAP	Pole Aerial Photography	UAS_RC	DEM from UAS data, corrected for refraction
PAP_HQ	DEM from High Quality Pole Aerial Photography data set (374 photos)		

Table 3: Overview of the data collected with each survey approach (Missing cell values (-) are either due to the information not being relevant for a specific approach or because information was not collected).

	TLS_AV G	TLS_M AX	PAP_HQ	PAP_LQ	UAS	
Survey date	7-8 July 2013	7-8 July 2013	8 July 2013	8 July 2013	6 July 2013	
Survey duration (approx. no. hours)	9	9	2	2	6	
Average camera height/range (m)	-	-	5	5	29	
Spatial coverage (m <sup>2</sup> )	7690	7690	859	859	4382	
Coverage efficiency (m <sup>2</sup> /hour)	854	854	430	430	730	
Exposed areas - All (% of total coverage)	-	-	82	82	91	
Submerged areas (% of total coverage)	-	-	18	18	9	
Exposed areas - All (% of total coverage) - vegetated	-	-	64	64	-	
Number of GCPs used	-	-	10	10	25	
Number of validation points exposed areas - vegetated	58	58	58	58	58	
Number of validation points exposed areas - non- vegetated	86	86	86	86	86	
Number of validation points collected in submerged areas	116	116	116	116	116	
Spatial Resolution (DEM) (m)	0.013	0.01	0.009	0.009	0.020	
Spatial Resolution (Orthophoto) (m)	-	-	0.002	0.002	0.010	
Number of photos collected	-	-	400	400	88	
Number of photos used	-	-	374	114	64	
Residual error (Mean)						
	x	0.009	0.009	-0.001	-0.0004	0.006
	y	0.009	0.009	-0.002	-0.0001	-0.007
	z	0.026	0.026	0.001	0.0002	0.022
Residual error (SD)						
	x	-	-	0.021	0.024	0.062
	y	-	-	0.029	0.029	0.043
	z	-	-	0.010	0.012	0.037

Table 4a. Comparison of DEM results from each surveying method with all ground validation data (GVPs). A gradual greyscale scheme is used to emphasize variation in the observed errors.

	All GVPs		Exposed (no vegetation)		Submerged		Vegetated	
	Whole site Mean Error	SD	Mean Error	SD	Mean Error	SD	Mean Error	SD
PAP_HQ	0.103	0.275	0.036	0.053	0.091	0.211	0.334	0.406
PAP_HQ_RC	0.082	0.280	0.041	0.070	0.047	0.216	0.334	0.406
PAP_LQ	0.037	0.189	0.049	0.070	0.057	0.184	0.187	0.281
TLS_AVG	0.123	0.214	0.006	0.107	0.123	0.195	0.295	0.254
TLS_MAX	0.135	0.223	0.017	0.128	0.129	0.198	0.323	0.255
UAS	0.049	0.148	0.038	0.107	0.050	0.095	0.177	0.191
UAS_RC	0.031	0.147	0.038	0.106	0.008	0.091	0.179	0.187

Legend: (m)

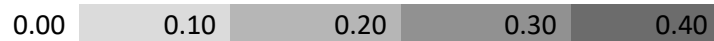


Table 4b. Comparison of DEM results from each surveying method with ground validation data, using GVPs at <5 m from GCPs only. A gradual greyscale scheme is used to emphasize the variation in the observed errors.

	GVPs <5 m from GCP		Exposed (no vegetation)		Submerged		Vegetated	
	Whole site Mean Error	SD	Mean Error	SD	Mean Error	SD	Mean Error	SD
PAP_HQ	0.085	0.180	0.013	0.028	0.082	0.104	0.283	0.297
PAP_HQ_RC	0.066	0.180	0.013	0.028	0.038	0.095	0.283	0.297
PAP_LQ	0.066	0.160	0.020	0.035	0.075	0.122	0.256	0.254
TLS_AVG	0.145	0.235	0.010	0.074	0.163	0.250	0.367	0.229
TLS_MAX	0.154	0.239	0.016	0.077	0.165	0.253	0.394	0.221
UAS	0.051	0.143	0.042	0.045	0.061	0.114	0.208	0.179
UAS_RC	0.029	0.142	0.042	0.046	0.011	0.111	0.208	0.178

Legend: (m)



Table 4c. Comparison of realigned DEM results from each surveying method with ground validation data, using all GVPs and GVPs at <5 m from GCPs only. A gradual greyscale scheme is used to emphasize the variation in the observed errors.

	All GVPs		Exposed (no vegetation)		Submerged		Vegetated	
	Whole site Mean Error	SD	Mean Error	SD	Mean Error	SD	Mean Error	SD
PAP_HQ	0.103	0.275	0.036	0.053	0.091	0.211	0.334	0.406
PAP_HQ_RC	0.082	0.280	0.041	0.070	0.047	0.216	0.334	0.406
PAP_LQ	0.037	0.189	0.049	0.070	0.057	0.184	0.187	0.281
TLS_AVG_GEOREF	0.133	0.228	0.038	0.191	0.120	0.197	0.298	0.247
TLS_MAX_GEOREF	0.156	0.263	0.073	0.293	0.129	0.203	0.330	0.247
UAS_GEOREF	0.078	0.240	0.001	0.261	0.062	0.189	0.223	0.237

	GVPs <5 m from GCP							
PAP_HQ	0.085	0.180	0.013	0.028	0.082	0.104	0.283	0.297
PAP_HQ_RC	0.066	0.180	0.013	0.028	0.038	0.095	0.283	0.297
PAP_LQ	0.066	0.160	0.020	0.035	0.075	0.122	0.256	0.254
TLS_AVG_GEOREF	0.147	0.230	0.018	0.082	0.162	0.249	0.364	0.212
TLS_MAX_GEOREF	0.161	0.248	0.046	0.184	0.163	0.248	0.375	0.212
UAS_GEOREF	0.073	0.222	0.045	0.081	0.090	0.248	0.260	0.211

Legend: (m)

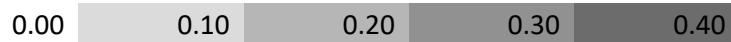


Table 5. DoD summary results (mean and standard deviation in metres) for selected combinations of DEMs. A gradual greyscale scheme is used to emphasize the variation in the observed errors.

Exposed (no vegetation)	PAP_HQ		UAS		UAS_GEOREF		TLS_AVG_GEOREF	
	Mean	SD	Mean	SD	Mean	SD	Mean	SD
PAP_LQ	-0.018	0.074						
UAS	-0.002	0.121						
TLS_AVG	0.042	0.138	0.042	0.133	0.041	0.200		
TLS_AVG_GEOREF	0.061	0.141	0.059	0.140	0.046	0.142		
TLS_MAX	0.054	0.157	0.054	0.139	0.028	0.197		
TLS_MAX_GEOREF	0.075	0.170	0.073	0.156	0.059	0.144	0.014	0.060

Submerged | PAP\_HQ | UAS | UAS\_GEOREF | TLS\_AVG\_GEOREF

	Mean	SD	Mean	SD	Mean	SD	Mean	SD
PAP_LQ	-0.027	0.116						
UAS	0.030	0.172						
TLS_AVG	0.024	0.186	0.053	0.086	0.059	0.119		
TLS_AVG_GEOREF	0.030	0.191	0.042	0.109	0.048	0.093		
TLS_MAX	0.030	0.189	0.060	0.091	0.067	0.133		
TLS_MAX_GEOREF	0.038	0.199	0.049	0.113	0.056	0.102	0.008	0.042

Vegetated	PAP_HQ		UAS		UAS_GEOREF		TLS_AVG_GEOREF	
	Mean	SD	Mean	SD	Mean	SD	Mean	SD
PAP_LQ	0.015	0.141						
UAS	0.140	0.285						
TLS_AVG	-0.049	0.289	0.088	0.166	0.029	0.210		
TLS_AVG_GEOREF	-0.014	0.245	0.127	0.187	0.067	0.166		
TLS_MAX	-0.011	0.290	0.128	0.173	0.069	0.206		
TLS_MAX_GEOREF	0.023	0.250	0.167	0.213	0.107	0.168	0.040	0.085

Legend (m):

-0.300	-0.200	-0.100	0.000	0.100	0.200	0.300	0.400
--------	--------	--------	-------	-------	-------	-------	-------

Table 6. Result of M3C2 cloud comparison tool (mean and standard deviation in metres) for selected combinations of point clouds. A gradual greyscale scheme is used to emphasize the variation in the observed errors. Cells with thick outlines contain a result that is notably different from the equivalent DoD result.

Exposed (no vegetation)	PAP_HQ		UAS	
	Mean	SD	Mean	SD
UAS	-0.007	0.140		
TLS	0.061	0.223	-0.007	0.153

Vegetated	PAP_HQ		UAS	
	Mean	SD	Mean	SD
UAS	-0.104	0.119		
TLS	0.018	0.213	0.094	0.125

## 9 Figures

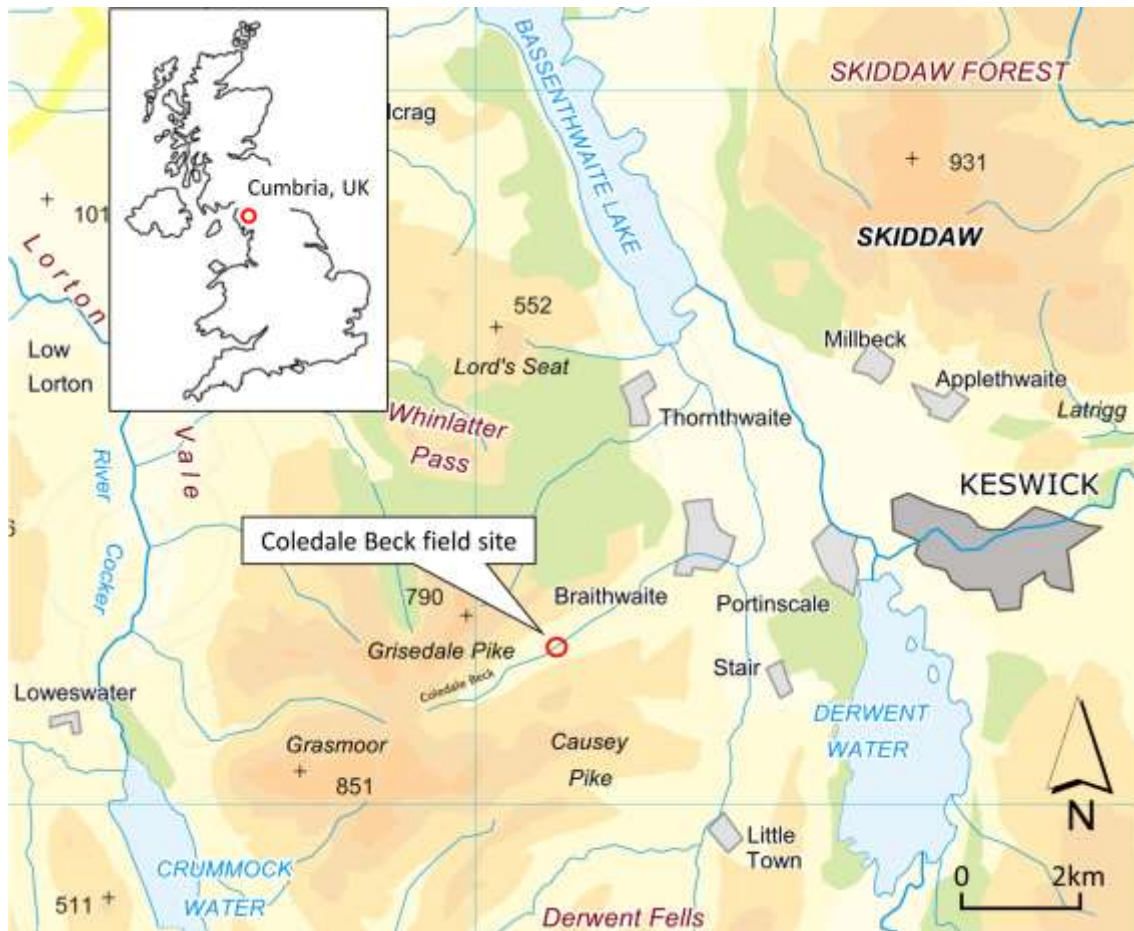


Figure 1: Location map of the Coledale Beck study site in Cumbria, UK. Grid reference NY 21291 22381. (Background map: © Crown Copyright and Database Right (2018). Ordnance Survey (Digimap Licence))





Figure 2 Photographic impressions of the geomorphological diversity of the field sites; (a) oblique perspective from ground level; (b+c) pole camera perspective.

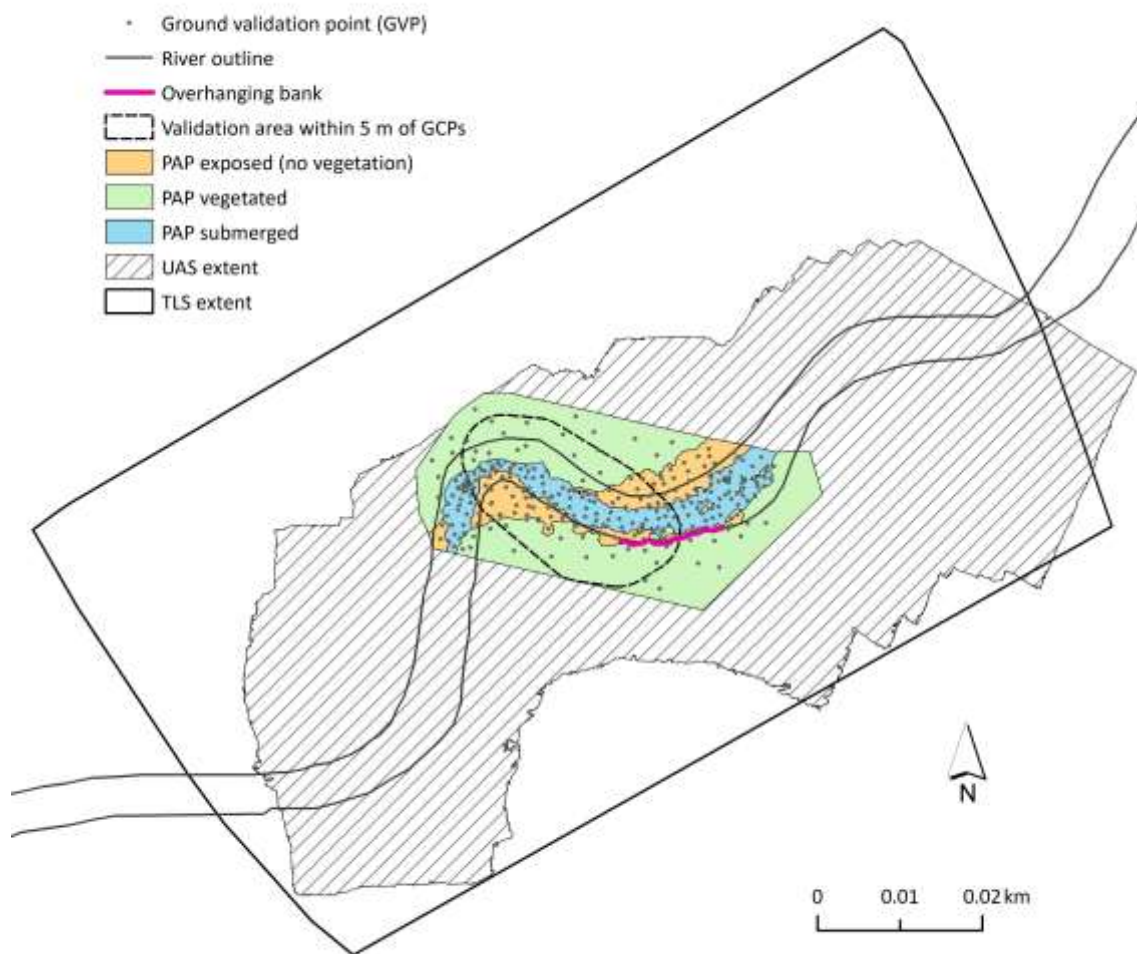


Figure 3: Extent of DEM models created from pole aerial photography (PAP), from images taken from a UAS and using a terrestrial laser scanner (TLS), including location of ground validation points (GVPs) and delineation of surface types.

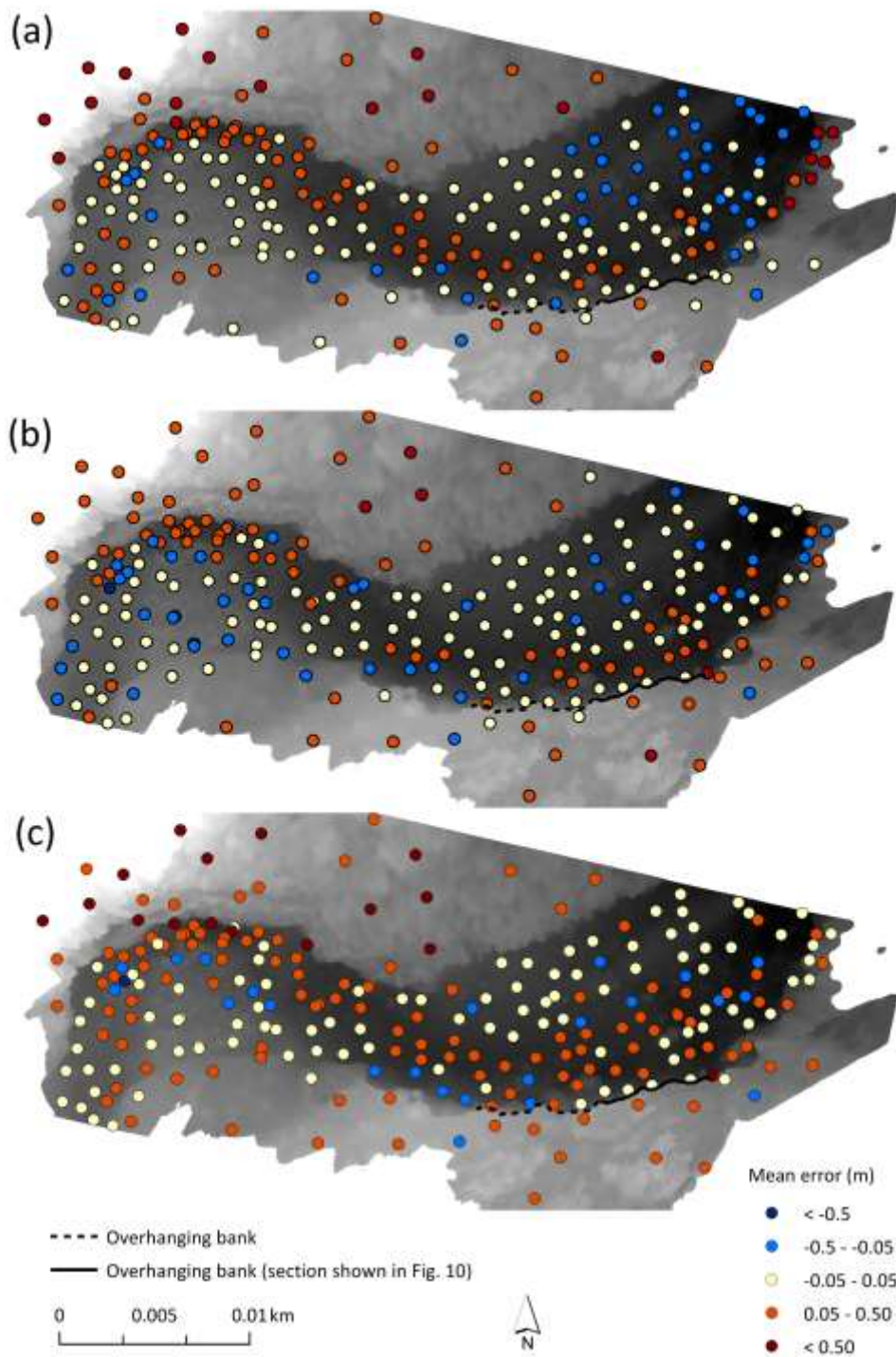


Figure 4: Distribution of error at ground validation points for the PAP\_HQ (a), UAS (b) and TLS\_AVG (c) DEMs.

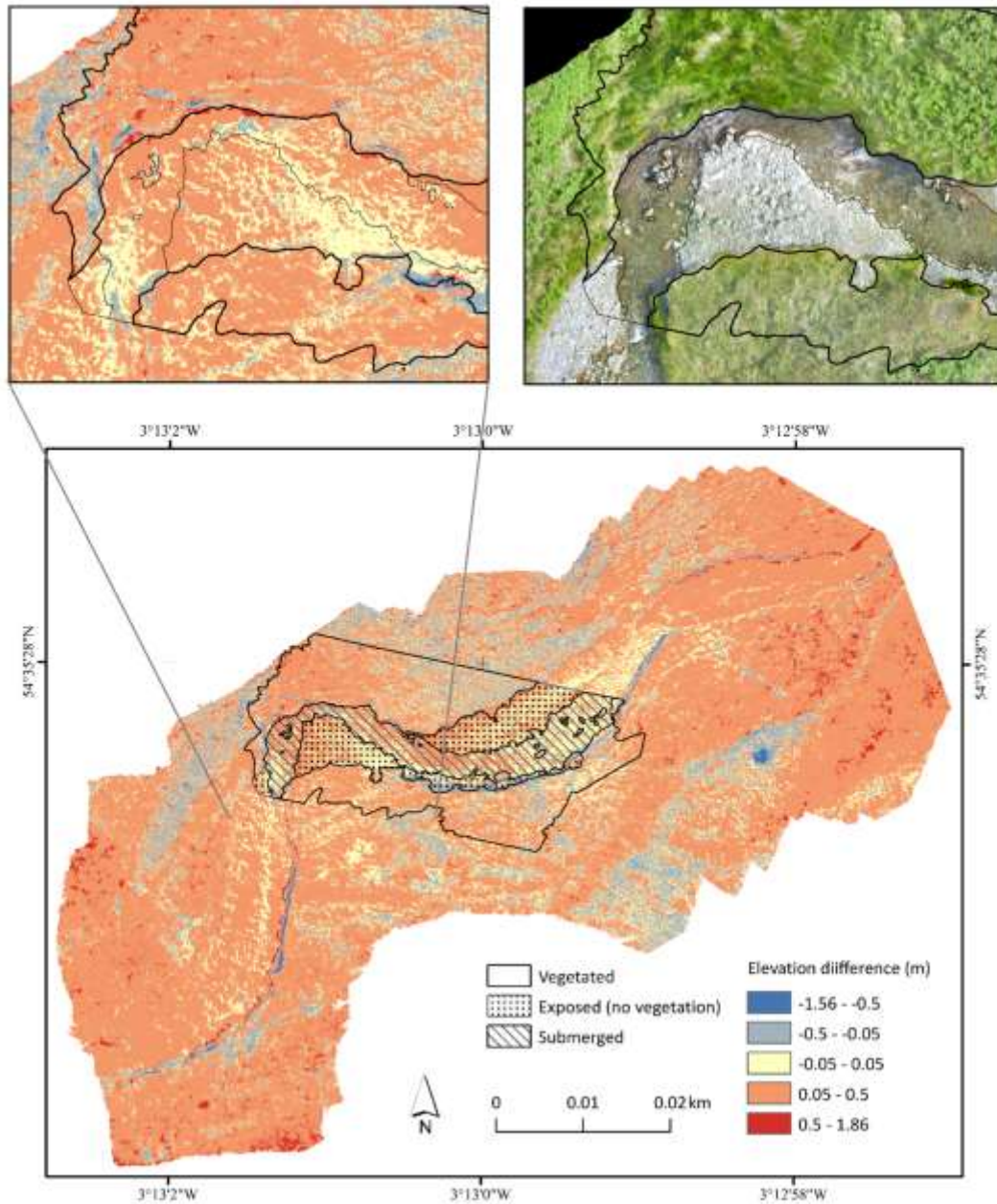


Figure 5: DoD between TLS\_AVG and UAS (orange-red: overestimated, light blue-blue: underestimated and yellow: < 0.05 m difference). Inset shows shadow effect around larger boulders and orthophoto segment of the same area for reference.

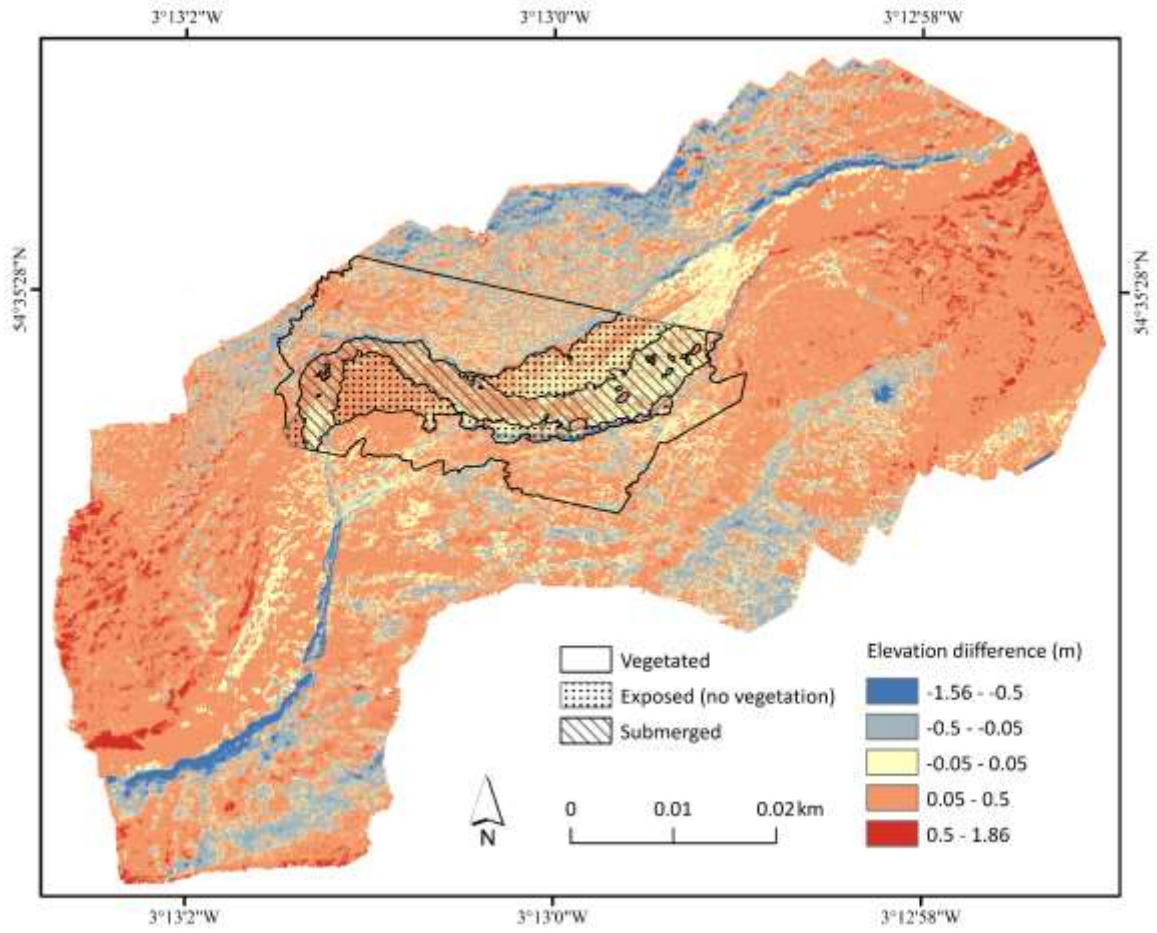


Figure 6: DoD between TLS\_AVG\_GEOREF and UAS\_GEOREF.

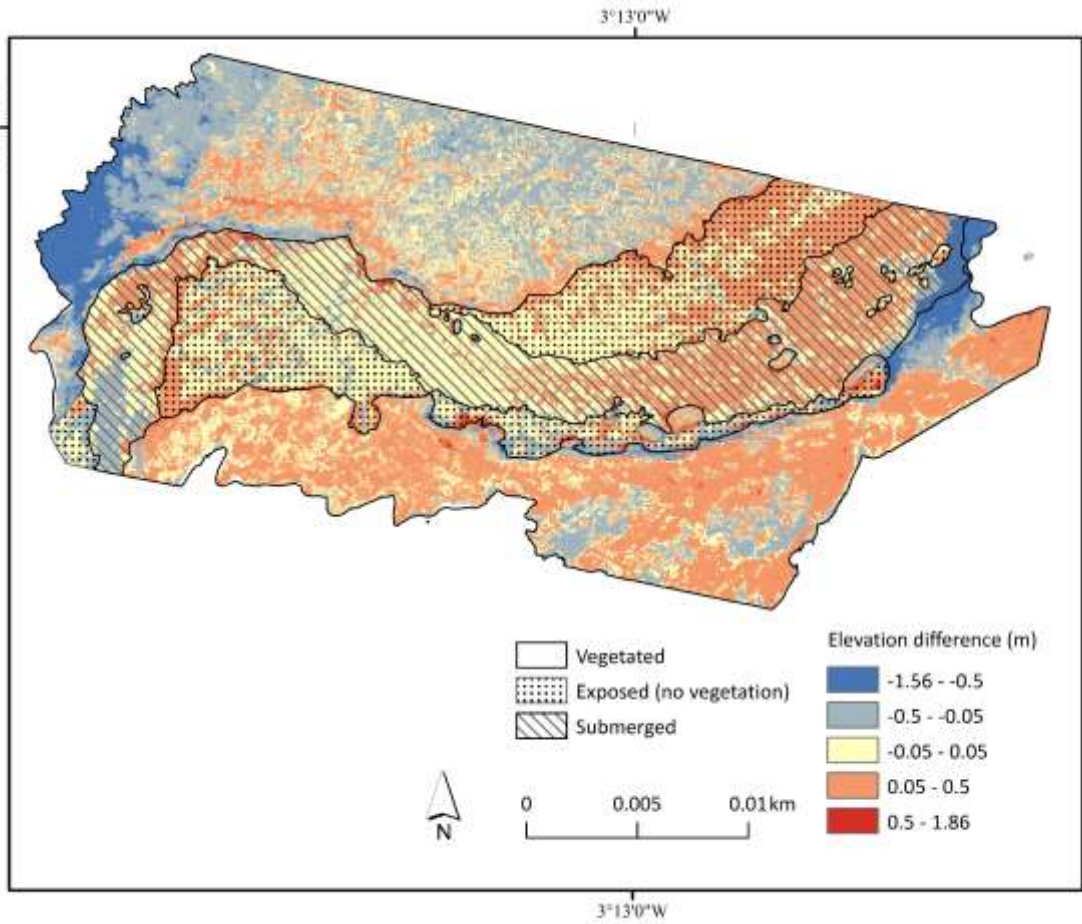


Figure 7: DoD between TLS\_AVG and PAP\_HQ.

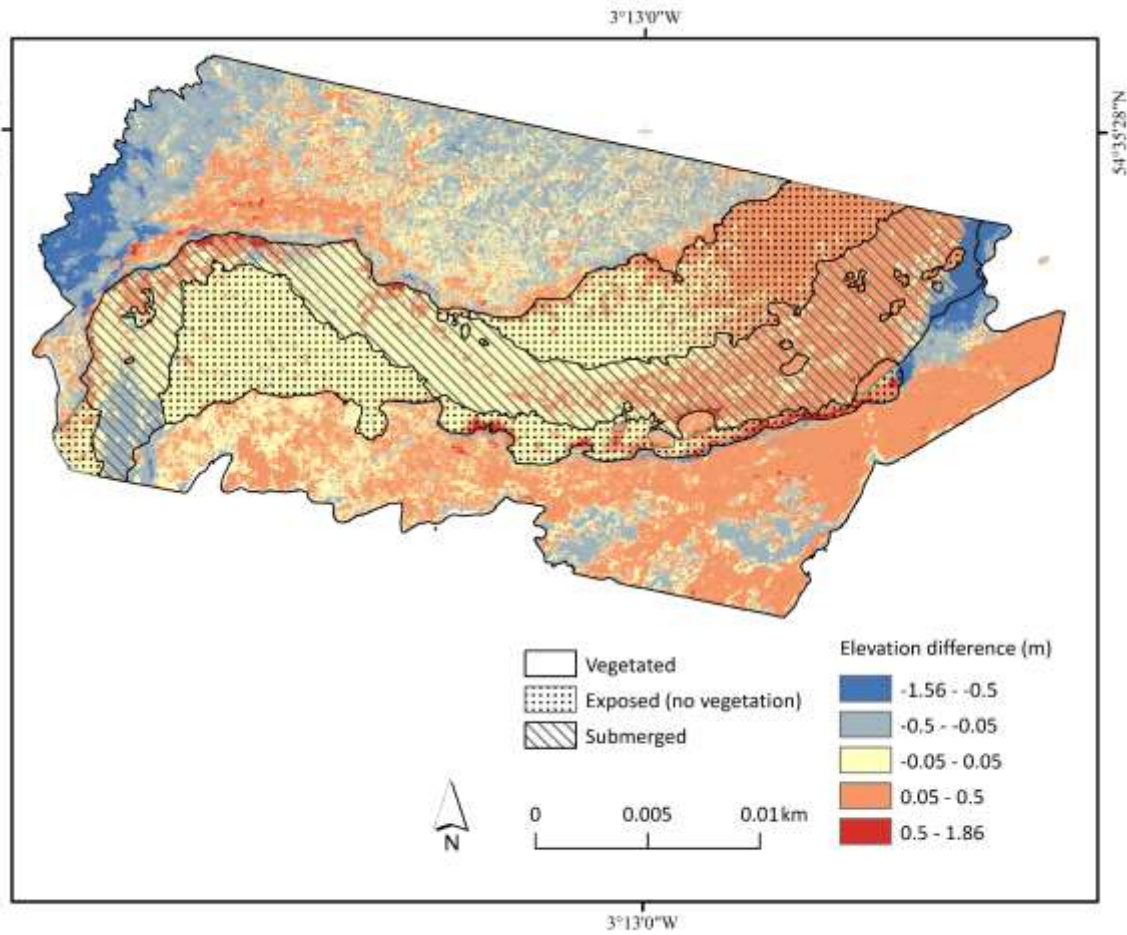


Figure 8: DoD between TLS\_AVG\_GEOREF and PAP\_HQ.

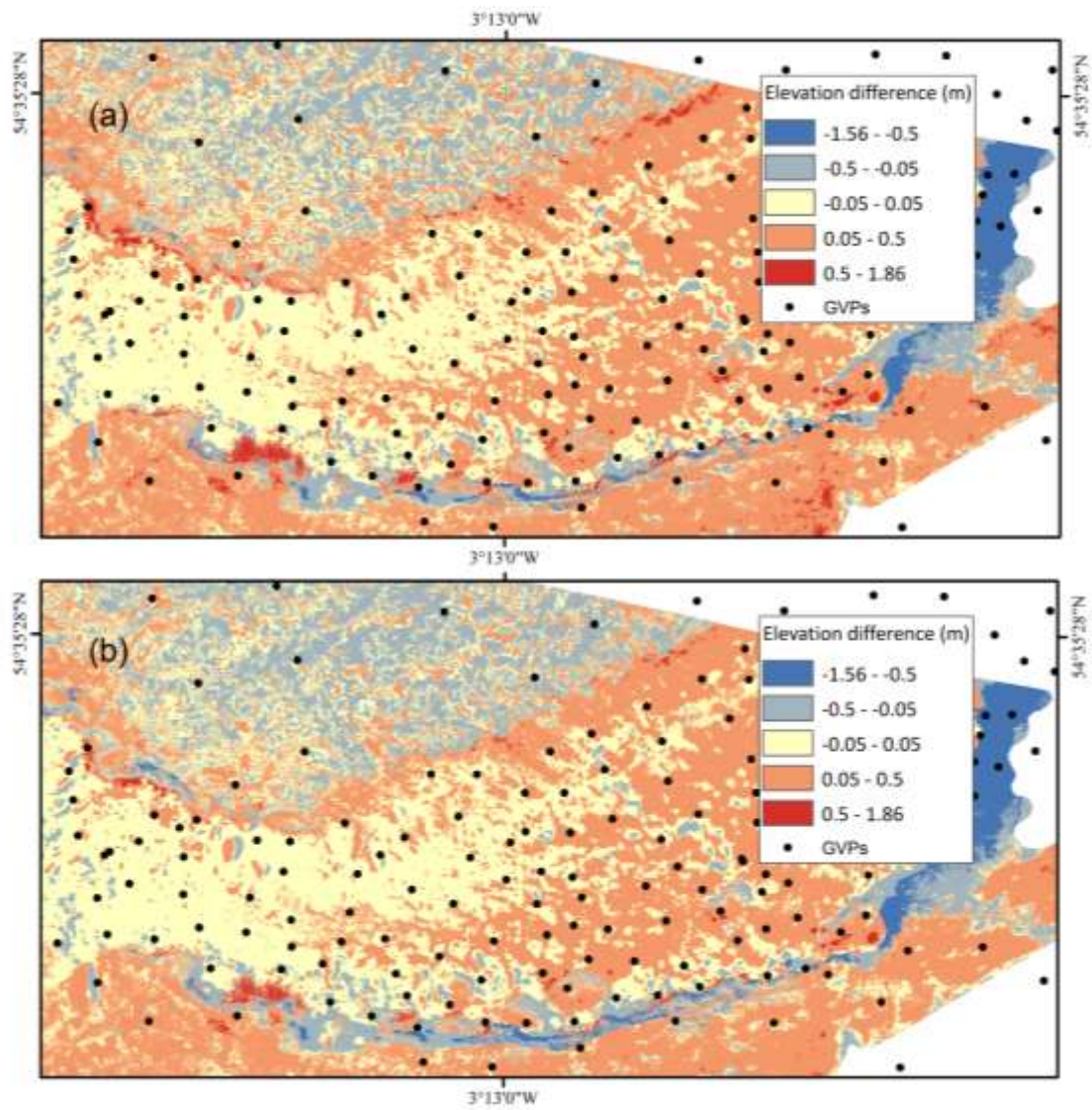


Figure 9: Close-ups of DoD between TLS\_MAX and PAP\_HQ (a) and between TLS\_AVG and PAP\_HQ (b).





Figure 10: PAP\_HQ model close-up illustrating a capacity to capture overhanging bank features. See Figures 2 and 3 for exact feature location. Orange line represents a 6.5 m section along the right riverbank. Arrow indicates flow direction.